High strain rate damage of Carrara marble

Mai-Linh Doan[1] and Andrea Billi[2]

Received 4 August 2011; revised 2 September 2011; accepted 2 September 2011; published 8 October 2011.

[1] Several cases of rock pulverization have been observed along major active faults in granite and other crystalline rocks. They have been interpreted as due to coseismic pervasive microfracturing. In contrast, little is known about pulverization in carbonates. With the aim of understanding carbonate pulverization, we investigate the high strain rate (c. 100 s^{-1}) behavior of unconfined Carrara marble through a set of experiments with a Split Hopkinson Pressure Bar. Three final states were observed: (1) at low strain, the sample is kept intact, without apparent macrofractures; (2) failure is localized along a few fractures once stress is larger than 100 MPa, corresponding to a strain of 0.65%; (3) above 1.3% strain, the sample is pulverized. Contrary to granite, the transition to pulverization is controlled by strain rather than strain rate. Yet, at low strain rate, a sample from the same marble displayed only a few fractures. This suggests that the experiments were done above the strain rate transition to pulverization. Marble seems easier to pulverize than granite. This creates a paradox: finely pulverized rocks should be prevalent along any high strain zone near faults through carbonates, but this is not what is observed. A few alternatives are proposed to solve this paradox. **Citation:** Doan, M.-L., and A. Billi (2011), High strain rate damage of Carrara marble, *Geophys. Res. Lett.*, *38*, L19302, doi:10.1029/2011GL049169.

1. Introduction

[2] Pulverized rocks have been recently identified near some major active faults [*Dor et al.*, 2006, 2009; *Mitchell et al.*, 2011] as a rare example of fault damage, where intense microfracturing occurred while the primary rock structure experienced a minimal distortion (i.e., no or minimal shear strain). Intense damage occurred at low shear strain and microfractures permeated the whole rock using original grain boundaries or crosscutting them, thus producing a very fine-grained material with most grains smaller than 1 mm.

[3] The origin of pulverized rocks is still debated. Their occurrence along major faults suggests a connection with fault mechanics and, in fact, experimental data suggest that pulverization is a marker of coseismic damage due to strong earthquakes [*Doan and Gary*, 2009]. Pulverized rocks may thus provide important clues to advance the understanding of earthquake physics and seismic faults [*Reches and Dewers*, 2005; *Wilson et al.*, 2005; *Dor et al.*, 2006; *Yuan et al.*, 2011].

[4] The knowledge of natural pulverized rocks is, however, still very limited under many aspects. For instance, known occurrences of pulverized rocks are so far limited to only a few sites and major faults (all strike-slip, with prominent bimaterial interfaces), namely along the San Andreas Fault system [*Wilson et al.*, 2005; *Dor et al.*, 2006; *Rockwell et al.*, 2009; *Wechsler et al.*, 2011], the Northern Anatolian Fault [*Dor et al.*, 2008], and the Arima-Takatsuki Fault [*Mitchell et al.*, 2011]. Interestingly, occurrence of pulverization is so far limited to a small number of lithologies, mainly crystalline rocks, with the exception of a sandstone outcrop along the San Andreas Fault [*Dor et al.*, 2009].

[5] In carbonate rocks, finely-comminuted fault rocks with grains smaller than 1 mm occur in high shear strain zones (i.e., the fault core [e.g., *Storti et al.*, 2003; *Billi and Storti*, 2004; *Billi*, 2005; *Agosta and Aydin*, 2006; *Frost et al.*, 2009]). In contrast, low-strain, poorly-distorted, fault-related breccias are relatively common, but always in low-strain zones (i.e., the damage zone) and usually with large grains (>1 cm) [*Billi et al.*, 2003], much larger than for the usual pulverized rocks (<1 mm). So far, the only exception is the carbonate fault rock observed in central Italy along a seismically-active normal fault cutting through shallow-water Mesozoic limestone, where finely comminuted rock (grains up to c. 1 cm in maximum size), interpreted as pulverized rock for the occurrence of apparently preserved layering, forms a 1-m-thick band running along the fault core on the footwall side [*Agosta and Aydin*, 2006]. The hangingwall is downthrown and buried so no information is available about a possible bimaterial interface effect. Moreover, the true origin of this rock (i.e., the pulverized limestone) has still to be conclusively ascertained by microscopic observations. Other reported cases of preserved carbonate rocks embedded within pulverized crystalline rocks [see *Dor et al.*, 2006, Figure 5] suggest a scarce propensity of carbonates to pulverization.

[6] To understand why carbonates seem so little prone to pulverization, we ran high strain rate testing of carbonate rocks in the laboratory. As sedimentary carbonates are very heterogeneous, we focused our first study of carbonate dynamic pulverization on the most homogeneous and crystalline variety of carbonate (i.e., the Carrara marble; Figure 1a). Dynamic loading was done with a Split Hopkinson Pressure Bar apparatus [*Chen and Song*, 2010] to record the uniaxial behavior of samples at strain rates on the order of 100 s^{-1}.

[7] After presenting the experimental method, we relate the evolution of strength and damage pattern to strain and strain rate. We discuss the experimental results in light of the microstructural damage, before concluding on the relevance of our study to seismic faults in carbonates.

2. Method

[8] Experiments were done using a Split Hopkinson Pressure Bar (SHPB) apparatus in the Laboratoire de Mécanique des Solides of the École Polytechnique, Palaiseau, France. Each sample was inserted between two bars impacted by a

[1]Institut des Sciences de la Terre, Université Joseph Fourier, Grenoble, France.
[2]IGAG, Consiglio Nazionale delle Ricerche, Rome, Italy.

0094-8276/11/2011GL049169

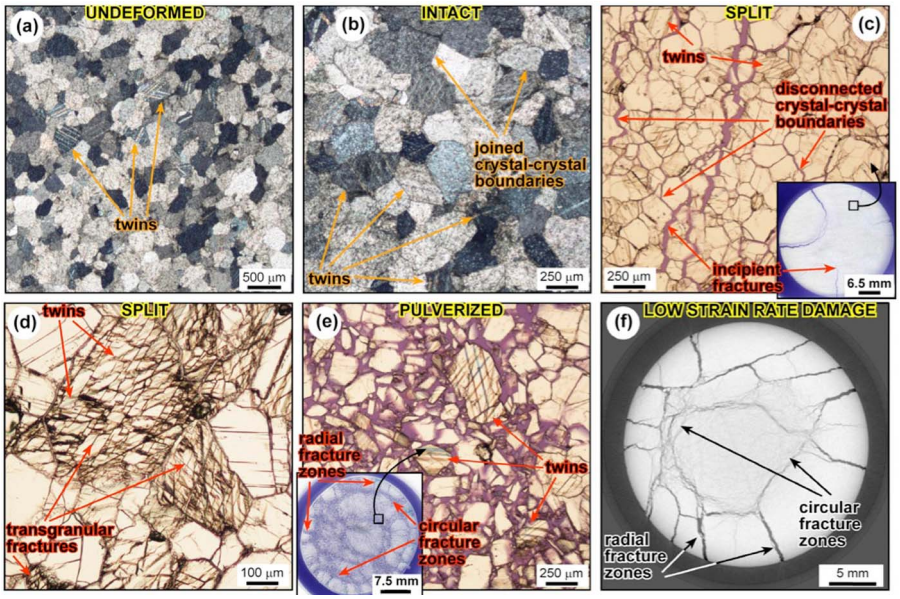

Figure 1. Microphotographs of Carrara marble samples. Figures 1b–1e are perpendicular to loading in the SHPB apparatus and Figure 1f is perpendicular to loading in the low strain rate apparatus. (a) Undeformed Carrara marble (crossed nicols). Note episodic calcite twinning. (b) Apparently intact sample M04 (crossed nicols). Note calcite twins and joined boundaries between crystals. (c) Split sample M16 (parallel nicols). Note a rather pervasive incipient disarticulation of crystal-crystal boundaries. Inset shows a thin-section parallel and close to the input surface of the cylindrical sample M16. The large microphotograph is taken from the thin-section in the inset. Note the occurrence of incipient radial fractures and incipient disarticulation of crystal-crystal boundaries. At least in places, calcite twinning preceded fracturing as shown by twins cut by fractures. (d) Enlargement from split sample M16 (parallel nicols). Note transgranular fractures cutting through twinned non-distorted grains. (e) Pulverized sample M01 (parallel nicols). Inset shows a thin-section parallel and close to the input surface of the cylindrical sample M01. Note the radial and circular main fracture zones affecting the thin-section. The large microphotograph is taken from the thin-section in the inset and shows a complete disarticulation of the crystal-crystal boundaries plus fractures breaking the original grains, some of which contain calcite twins. (f) Damage pattern of Carrara marble subjected to low strain deformation. Note large strain (fractures) occurred under low strain rate.

striker bar arriving at a known velocity. The dimensions of the bars (length: 3 m; diameter: 4 cm) are so that the propagation of elastic waves in the bars is mainly one-dimensional [*Gama et al.*, 2004]. Using the first mode solution of the Pochhammer-Chree equation of wave propagation in bars, forces and displacements applied to the bar ends were retrieved from strain gauges glued on the bars. We checked that the forces were identical at the input and output bars to ensure that the sample was homogenously loaded. We could then derive the history of stress, strain, and strain rate experienced by the sample. Due to their short duration, experiments were not servo-controlled. The loading duration is related to the length of the striker bar. Hence, strain tends to increase with strain rate. We compensate for this drawback of the SHPB apparatus by changing the material of the bars and by varying the length of the striker.

Table 1. Summary of Experimental Data

Sample	Length (mm)	Diameter (mm)	Max. True Stress (MPa)	Max True Strain Rate (s^{-1})	Max True Strain (%)	Dissipated Volumetric Energy (MJ/m^3)	Rubber Jacket	Post-experiment State[a]
M01	28.06	25.62	121	202	3.38	2.03	yes	pulverized (red)
M02	27.65	25.64	110	209	3.64	1.88	yes	pulverized (red)
M03	28.65	25.97	103	120	1.82	1.18	yes	pulverized (red)
M04	28.75	25.59	66	42	0.38	0.12	yes	intact (green)
M05	28.31	25.66	101	140	2.19	1.39	yes	pulverized (red)
M07	28.64	25.61	110	205	3.49	1.74	no	pulverized (red)
M08	28.27	25.67	108	131	1.37	1.09	yes	pulverized (red)
M10	28.12	25.68	35	16	0.15	0.02	yes	intact (green)
M12	28.19	25.58	106	84	0.60	0.32	yes	intact (green)
M13	28.49	25.62	99	86	0.73	0.45	yes	split (blue)
M15	28.66	25.66	79	116	1.86	1.05	no	pulverized (red)
M16	28.22	25.63	110	91	0.98	0.74	no	split (blue)
M17	28.46	25.68	127	35	0.69	0.51	no	split (blue)
M18	27.74	25.69	129	68	1.66	1.36	no	pulverized (red)

[a]Colors in parentheses correspond to the classification of final macroscopic damage of Figure 3.

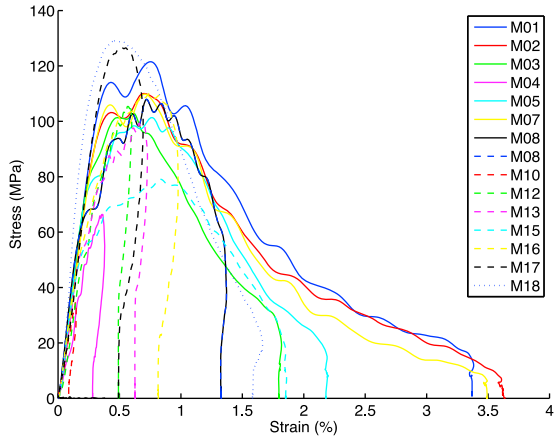

Figure 2. Experimental strain-stress curves of all samples. The peak stress is consistent for all the sample. The Young modulus is also similar, around 10 GPa.

[9] We deformed 14 cylindrical samples (length and diameter: c. 25 mm; Table 1) of Carrara marble. The fine grain size of the Carrara marble (c. 0.2–0.4 mm; Figure 1) is much smaller than the dimension of the sample. Some samples were jacketed with a rubber jacket to preserve and study the post-experiment deformation fabric. We then impregnated these samples with an indurative epoxy resin and cut them to analyze their fabric under an optical microscope (Figure 1).

[10] We also conducted a quasi-static uniaxial compressive test on a jacketed sample using a Schenk press located at the 3SR Laboratory in Grenoble, France, with a strain rate of 10^{-5} s^{-1} only. We used also the X-Ray CT scan tomography of the same laboratory to microstructurally investigate the sample after the quasi-static test (Figure 1f). Details on the scanning apparatus and processing of data from the X-Ray CT Scan are similar to *Lenoir et al.* [2007].

3. Results

[11] With increasing strain and strain rate, we obtained three main post-experimental deformation fabrics (Table 1): (1) strongly cohesive, apparently intact samples (i.e., apparently intact or with one or two incipient fractures at the most; Figure 1b), (2) poorly cohesive, split samples (i.e., with some main fractures splitting the sample in a few large fragments; Figures 1c and 1d), and (3) uncohesive, pulverized samples (i.e., with diffuse microfractures and most fragments less than 1 mm in size; Figure 1e), where the distance between microfractures is about 500 μm.

[12] Before failure, the samples experienced similar elastic loading phases (Figure 2), with a Young's modulus of 20 GPa. The Young's modulus is not sensitive to strain rate. Strength of the sample is about 100 MPa, similar to the strength recorded in the literature for low strain rate experiments on Carrara marble at room temperature and 5 MPa of confining pressure [*Fredrich et al.*, 1989]. Below the 100 MPa threshold, we do not see any macroscopic diffuse damage (Figures 1 and 3 and Table 1). Note that, in all experiments, there is a permanent strain (Figure 2) suggesting that inelastic processes occurred (e.g., twinning and microfracturing; Figure 1).

[13] Diagrams of strain and strain rate vs. the maximum stress attained in the samples as well as the diagram of strain vs. the energy dissipated in the experiments are shown in Figure 3. These experimental results show that, although an approximate trend toward pulverization with increasing strain rate is visible (see, for instance, results from samples M01, M02, M03, M07, M08, M05, and M15 in Table 1), unlike granite [*Doan and Gary*, 2009; *Yuan et al.*, 2011], in the Carrara marble, the transition between split and pulverized

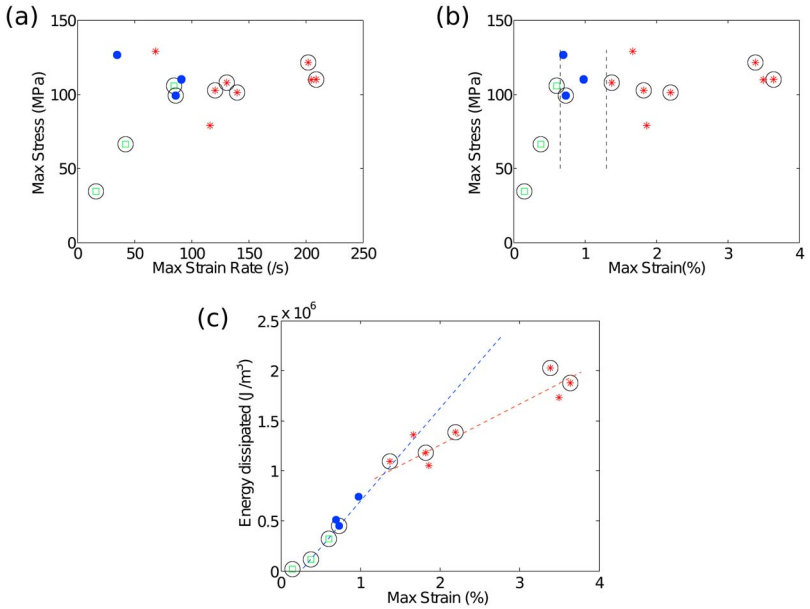

Figure 3. Phase diagrams of the macroscopic damage patterns. (a) Maximum strain rate vs. maximum stress. (b) Maximum strain vs. maximum stress. (c) Dissipated energy vs. maximum stress. Green squares, blue circles, and red asterisks indicate, respectively, apparently intact, split, and pulverized samples. Jacketed samples are indicated with a circle surrounding the damage symbol.

rocks with strain rate is not obvious (Figure 3a). Sample M18, for instance, is pulverized for a strain rate of 68 s^{-1}, whereas sample M13 is simply split by some main macroscopic fractures for a strain rate of 86 s^{-1} (Table 1). In contrast, the post-experiment damage pattern seems well correlated with the total strain accumulated (Figure 3b) rather than strain rate (Figure 3a). Macroscopic fractures appear in split samples when strain exceeds 0.65%, whereas intense microscopic fragmentation (pulverized samples) appears at strains beyond 1.3%. There is, therefore, a narrow interval during which a few macroscopic fractures develop (the interval between vertical dashed lines in Figure 3b). For higher strains, microscopic fractures pervade samples up to their pulverization (strain > 1.3%) by primarily using crystal-crystal boundaries and, more rarely, cutting through crystals (Figure 1). Hence, marble pulverization is primarily controlled by strain rather than strain rate (Figure 3).

[14] In Figure 3, samples that were jacketed are plotted with circled symbols. Their final macroscopic state is the same as the final state of unjacketed samples loaded under the same conditions. Their strain-stress curve is also similar (Figure 2). Hence, jacketing has no effect on the mechanical results (Figure 3). We can safely analyze the sample microstructure and generalize to the whole dataset. The pertinence of our experimental results to explain the natural pulverization of carbonates is discussed in the following sections.

4. Damage Processes

[15] Carbonate rocks display both ductile and brittle behavior even at low confining pressure [*Evans and Kohlstedt*, 1995]. In our samples, calcite twinning (crystal-plastic deformation) is very moderate even in finely pulverized samples (Figure 1e). Moreover, limited twinning is present also in the undeformed marble (Figure 1a). Hence, plastic energy by twinning is not the main damage process and energy sink in our high strain rate experiments, where, in contrast, fractures play a major role in damage formation (Figure 1) and are most likely the main energy sink.

[16] In the apparently intact samples, the crystal-crystal boundaries appear (under the optical microscope) tightly joined (Figure 1b). In contrast, the same boundaries start to be diffusively disconnected in the split samples (Figure 1c) and become totally disconnected in the pulverized samples, where crystals are split apart from each other, and, in places, transgranular fractures split the original crystals into multiple subgrains (Figure 1e). In some cases, twinning predates fracturing (Figure 1c), whereas in other cases, fractures occur without shearing the pre-existing twins (Figure 1d).

[17] Without confining pressure, the sample splits naturally into several radial fractures. Figure 1c shows that the incipient fractures are radial fractures nucleated from the sample edge, a free surface where the inertial confinement effects [*Forrestal et al.*, 2004] are small. Tensional strength of rock is smaller than the compressional strength [*Jaeger et al.*, 2007] and radial pattern of tensile cracks forms finally. Such pattern has been also observed through X-Ray CT Scan on low strain rate experiments on sand [*Desrues et al.*, 1996] and sandstone [*Bésuelle et al.*, 2003]. This is not what is observed in pulverized samples of Carrara marble, where a new pattern of concentric fractures develops especially at high strain rates (Figure 1d). Several fractures propagate stress-shadowing each other, a process theoretically predicted by statistical theory of high strain rate damage [*Hild et al.*, 2003].

[18] The pulverized samples finally experience very large lateral expansion. For instance, the final diameter of sample M01 (Figure 1e) is about 3 cm (compared to the initial diameter of 2.5 cm), corresponding to a lateral expansion of 20%, which is enormous compared to the final uniaxial strain experienced by this sample (~3.4%; Table 1). It means that the sample, once pulverized, is not cohesive anymore and, therefore, centrifugal motion of grains is favored rather than creating new fractures across the grains. This inference is also supported by energy dissipation data (Figure 3c) as demonstrated below.

[19] In order to understand the energy related to damage mechanism, we estimate dissipated energy during loading by computing the quantity $\int_0^\infty \sigma\,\dot{\varepsilon}\,dt$. This quantity corresponds to the area below the stress-strain curves of Figure 2. The way dissipated energy evolves with strain or strain rate depends on the microphysics of damage. Figure 3c shows the dissipated energy vs. strain. Below a strain of 1.3%, both the intact and split samples align along the same line, with a slope of 103 MJ/m^3. It indicates that the damage mechanism is predominantly proportional to strain, suggesting an incremental damage. For pulverized samples, with strain above 1.3%, the data align with a slope of only 44 MJ/m^3. This smaller slope means that it is easier to further accommodate strain once rocks get pulverized. In other words, in Figure 3c, with increasing strain, samples switched from a cohesive "rock-like" behavior (steep slope) to a granular "gouge-like" behavior (gentle slope) [*Ben-Zion et al.*, 2011].

5. Application to Faults

[20] The above-discussed experimental results lead us to a few preliminary inferences about high strain rate damage in carbonates along seismic faults. In marble, to obtain the same degree of damage and fine grains as found in natural pulverized crystalline rocks [e.g., *Dor et al.*, 2006], strain larger than 1.3% is needed for a strain rate of about 100 s^{-1} (Figure 3). At low strain rate, uniaxial quasi-static testing of sample M14 up to a total strain of 3% gave a split samples, with a large number of fractures, but not a diffuse microfracturing throughout the entire sample (Figure 1f). This result confirms that pulverization along faults is a high strain rate feature, perhaps a coseismic marker. Then, what are the conditions for pulverization of Carrara marble during an earthquake? Our experimental results show that a minimum strain of 1.3% at about 100 s^{-1} is necessary (Figure 3b). Let us assume subshear propagation along a mode II rupture at constant velocity. We assume a pure elastic case, not taking into account any viscoelastic behavior within the process zone at the fracture tip. We use the same formulas as *Reches and Dewers* [2005] and *Doan and Gary* [2009], with a critical stress intensity factor K_{II} equal to 30 MPa $m^{1/2}$, as in *Reches and Dewers* [2005], and typical Lamé coefficients $\mu = \lambda = 4$ GPa, so that the Young modulus is 10 GPa as for our intact Carrara marble (Figure 2). We then obtain Figure 4, which shows that strain rate of 100 s^{-1} is attainable at distances from the fault core lower than 25 cm. The elastic properties of rock from the damage zone around a fault can be down to 50% lower than the protolith [*Faulkner et al.*, 2006; *Lewis and Ben-Zion*, 2010], in which case high

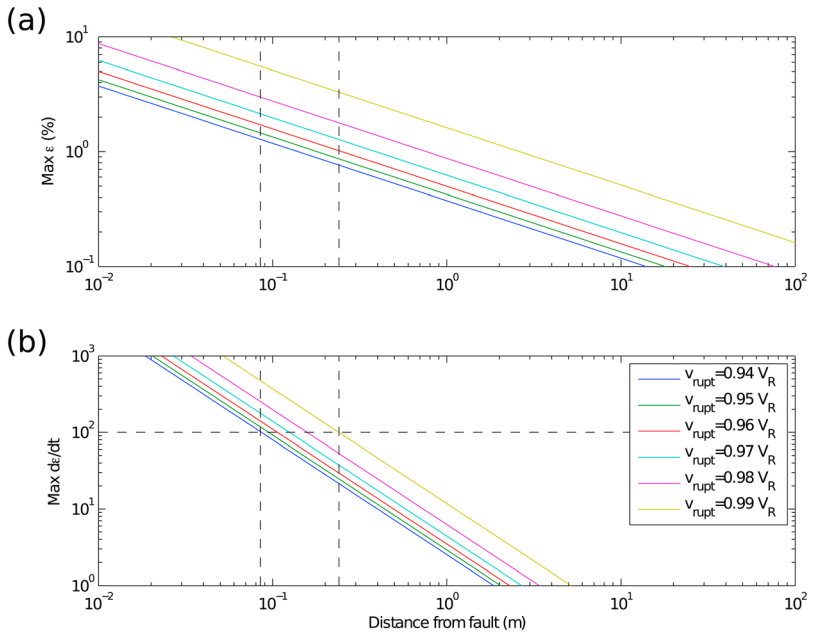

Figure 4. (a) Maximum strain and (b) strain rate experienced during an earthquake by a sample, depending on its distance to fault core. We assumed a subshear rupture of constant velocity v_{rupt}, proportional to the Rayleigh wave speed v_R. We used linear elastic fracture mechanics formalism, with critical stress intensity factor K_{II} equal to 30 MPa $m^{1/2}$, as by *Reches and Dewers* [2005], and typical Lamé coefficients $\mu = \nu = 4$ GPa, corresponding to Young modulus of 10 GPa, as in Figure 2. Dashed lines in the distance vs. maximum strain rate diagram delimit the range of distances from the fault core where a strain rate of 100 s^{-1} is attained. At this distance, strain compatible with the limit strain of Figure 3 is attainable. Hence, pulverization of limestone is possible very close to the fault for a subshear rupture of constant velocity.

strain rate can be reached a little farther from the fault zone (for instance, for $\mu = \lambda = 1$ GPa, a strain rate of 100 s^{-1} is attainable up to 40 cm away from the fault core; see auxiliary material).[1] This distance from the principal slip surface (40 cm) is usually well within the high shear strain zone (fault core) both in crystalline and in carbonate rocks [e.g., *Chester et al.*, 1993; *Frost et al.*, 2009]. Hence, it is probable that so close to the fault core, rock pulverization would be soon overprinted by the shear deformation leading to fault gouge development. This could be the case, in part, of the pulverized carbonate rocks signaled by *Agosta and Aydin* [2006] in central Italy. As pulverized rocks have been so far observed several tens of meters away from the fault core [*Dor et al.*, 2006, 2009], exceptional earthquakes, like supershear earthquakes [*Doan and Gary*, 2009] or a sudden acceleration of the rupture front must be invoked to reach pulverizing high strain rates so far from fault cores.

6. Conclusions

[21] In this paper, we presented how Carrara marble is damaged under uniaxial loading at high strain rate (c. 100 s^{-1}). At such strain rate, the transition from localized to diffuse damage is controlled by strain rather than strain rate and pulverization happens as soon as a strain above 1.3% is reached (Figure 3). This propensity for getting diffuse damage is paradoxical as pulverization is scarcely observed within carbonate rocks. To overstep this paradox, several explanations may be proposed. One is the fact that the Carrara marble may not be so representative of sedimentary marine limestone, which is the main carbonate lithotype affected by faults in the crust [*Billi et al.*, 2003; *Agosta and Aydin*, 2006; *Woodcock and Mort*, 2008]. An alternative explanation may simply be that carbonate pulverization occurs very close to fault cores (Figure 4), where, subsequently, shear deformation masks all pulverization effects. In the case of bimaterial faults, the dissymmetry in elastic properties on each side of the fault leads to a weaker loading on the weaker side [*Ben-Zion and Andrews*, 1998]. More generally, damage can also affect the strength of the material. Experiments on granite, for instance, show that pulverizing rocks is easier as rocks accumulate damage through successive earthquakes (M.-L. Doan and V. d'Hour, Effect of initial damage on rock pulverization, submitted to *Journal of Structural Geology*, 2011). The efficiency of healing in carbonates at shallow depths [*Renard et al.*, 2000, *Hausegger et al.*, 2010] may explain the preserved carbonate outcrops observed within pulverized granite, as in the Lake Hughes area along the San Andreas Fault [*Dor et al.*, 2006]. Hence, carbonate rocks may be preserved when juxtaposed with granite. In any case, the discussed paradox calls for further investigation on high strain rate damage of carbonates.

[22] **Acknowledgments.** We warmly thank Gérard Gary for allowing us to work on the Split Hopkinson Pressure Bars of Ecole Polytechnique, and for providing much advice on experimental issues. We thank Mimmo (Petrolab) for thin-sections, The experiments were performed with the equipment of Pascal Charrier and Jacques Desrues (3SR laboratory) for X-Ray tomography of low strain-rate sample, and Jean-Benoit Toni (3SR laboratory) for the low strain rate experiment. We acknowledge funding from INSU 3F and UJF TUNES programs. We thank Yehuda Ben-Zion, Jacques Desrues and Gérard Gary for improving earlier versions of the manuscript. We

[1] Auxiliary materials are available in the HTML. doi:10.1029/2011GL049169.

thank Erik Frost for his review that enabled us improve our text about the damage around carbonate faults.

[23] The Editor thanks Erik Frost for his assistance in evaluating this paper.

References

Agosta, F., and A. Aydin (2006), Architecture and deformation mechanism of a basin-bounding normal fault in Mesozoic platform carbonates, central Italy, *J. Struct. Geol.*, *28*, 1445–1467, doi:10.1016/j.jsg.2006.04.006.

Ben-Zion, Y., and D. J. Andrews (1998), Properties and implication of dynamic rupture along a material interface, *Geol. Soc. Am. Bull.*, *88*, 1084–1094.

Ben-Zion, Y., K. A. Dahmen, and J. T. Uhl (2011), A unifying phase diagram for the dynamics of sheared solids and granular materials, *Pure Appl. Geophys.*, doi:10.1007/s00024-011-0273-7.

Bésuelle, P., P. Baud, and T.-F. Wong (2003), Failure mode and spatial distribution of damage in Rothbach sandstone in the brittle-ductile transition, *Pure Appl. Geophys.*, *160*, 851–868, doi:10.1007/PL00012569.

Billi, A. (2005), Grain size distribution and thickness of breccia and gouge zones from thin (<1 m) strike-slip fault cores in limestone, *J. Struct. Geol.*, *27*, 1823–1837, doi:10.1016/j.jsg.2005.05.013.

Billi, A., and F. Storti (2004), Fractal distribution of particle size in carbonate cataclastic rocks from the core of a regional strike-slip fault zone, *Tectonophysics*, *384*, 115–128, doi:10.1016/j.tecto.2004.03.015.

Billi, A., F. Salvini, and F. Storti (2003), The damage zone-fault core transition in carbonate rocks: Implications for fault growth, structure and permeability, *J. Struct. Geol.*, *25*, 1779–1794, doi:10.1016/S0191-8141(03)00037-3.

Chen, W., and B. Song (2010), *Split Hopkinson (Kolsky) Bar: Design, Testing and Applications*, Springer, Berlin.

Chester, F. M., J. Evans, and R. Biegel (1993), Internal structure and weakening mechanisms of the San Andreas Fault, *J. Geophys. Res.*, *98*, 771–786, doi:10.1029/92JB01866.

Desrues, J., R. Chambon, M. Mokni, and F. Mazerolle (1996), Void ratio evolution inside shear bands in triaxial sand specimens studied by computed tomography, *Geotechnique*, *46*, 529–546, doi:10.1680/geot.1996.46.3.529.

Doan, M. L., and G. Gary (2009), Rock pulverization at high strain rate near the San Andreas Fault, *Nat. Geosci.*, *2*, 709–712, doi:10.1038/ngeo640.

Dor, O., Y. Ben-Zion, T. K. Rockwell, and J. Brune (2006), Pulverized rocks in the Mojave section of the San Andreas Fault Zone, *Earth Planet. Sci. Lett.*, *245*, 642–654, doi:10.1016/j.epsl.2006.03.034.

Dor, O., C. Yildrim, T. K. Rockwell, Y. Ben-Zion, O. Emre, M. Sisk, and T. Y. Duman (2008), Geological and geomorphologic asymmetry across the rupture zones of the 1943 and 1944 earthquakes on the North Anatolian Fault: possible signals for preferred earthquake propagation direction, *Geophys. J. Int.*, *173*, 483–504.

Dor, O., J. S. Chester, Y. Ben-Zion, J. Brune, and T. K. Rockwell (2009), Characterization of damage in sandstones along the Mojave section of the San Andreas Fault: Implications for the shallow extent of damage generation, *Pure Appl. Geophys.*, *166*, 1747–1773, doi:10.1007/s00024-009-0516-z.

Evans, B., and D. L. Kohlstedt (1995), Rheology of rocks, in *Rock Physics and Phase Relation: A Handbook of Physical Constants*, *AGU Ref. Shelf*, vol. 3, edited by T. J. Ahrens, pp. 148–165, AGU, Washington, D. C.

Faulkner, D. R., T. M. Mitchell, D. Healy, and M. J. Heap (2006), Slip on 'weak' faults by the rotation of regional stress in the fracture damage zone, *Nature*, *444*, 922–925, doi:10.1038/nature05353.

Forrestal, M. J., T. W. Wright, and W. Chen (2004), The effect of radial inertia on brittle samples during the split Hopkinson pressure bar test, *Int. J. Impact Eng.*, *34*, 405–411.

Fredrich, J. T., B. Evans, and T.-F. Wong (1989), Micromechanics of the brittle to plastic transition in Carrara marble, *J. Geophys. Res.*, *94*, 4129–4145, doi:10.1029/JB094iB04p04129.

Frost, E., J. Dolan, C. Sammis, B. Hacker, J. Cole, and L. Ratschbacher (2009), Progressive strain localization in a major strike-slip fault exhumed from midseismogenic depths: Structural observations from the Salzach-Ennstal-Mariazell-Puchberg fault system, Austria, *J. Geophys. Res.*, *114*, B04406, doi:10.1029/2008JB005763.

Gama, B. A., S. L. Lopatnikov, and J. W. Gillespie Jr. (2004), Hopkinson bar experimental technique: A critical review, *Appl. Mech. Rev.*, *57*, 223–250, doi:10.1115/1.1704626.

Hausegger, S., W. Kurz, R. Rabitsch, E. Kiechl, and F.-J. Brosch (2010), Analysis of the internal structure of a carbonate damage zone: Implications for the mechanisms of fault breccia formation and fluid flow, *J. Struct. Geol.*, *32*, 1349–1362, doi:10.1016/j.jsg.2009.04.014.

Hild, F., C. Denoual, P. Forquin, and X. Brajer (2003), On the probabilistic-deterministic transition involved in a fragmentation process of brittle material, *Comput. Struct.*, *81*, 1241–1253, doi:10.1016/S0045-7949(03)00039-7.

Jaeger, J., N. G. W. Cook, and R. Zimmerman (2007), *Fundamentals of Rock Mechanics*, 4th ed., Blackwell, Oxford, U. K.

Lenoir, N., M. Bornert, J. Desrues, P. Bésuelle, and G. Viggiani (2007), Volumetric digital image correlation applied to X-ray microtomography images from triaxial compression tests on argillaceous rock, *Strain*, *43*, 193–205, doi:10.1111/j.1475-1305.2007.00348.x.

Lewis, M. A., and Y. Ben-Zion (2010), Diversity of fault zone damage and trapping structures in the Parkfield section of the San Andreas Fault from comprehensive analysis of near fault seismograms, *Geophys. J. Int.*, *183*, 1579–1595, doi:10.1111/j.1365-246X.2010.04816.x.

Mitchell, T. M., Y. Ben-Zion, and T. Shimamoto (2011), Pulverized fault rocks and damage asymmetry along the Arima-Takatsuki Tectonic Line, Japan, *Earth Planet. Sci. Lett.*, *308*, 284–297, doi:10.1016/j.epsl.2011.04.023.

Reches, Z., and T. A. Dewers (2005), Gouge formation by dynamic pulverization during earthquake rupture, *Earth Planet. Sci. Lett.*, *235*, 361–374, doi:10.1016/j.epsl.2005.04.009.

Renard, F., J.-P. Gratier, and B. Jamtveit (2000), Kinetics of crack-sealing, intergranular pressure solution, and compaction around active faults, *J. Struct. Geol.*, *22*, 1395–1407, doi:10.1016/S0191-8141(00)00064-X.

Rockwell, T., M. Sisk, G. Girty, O. Dor, N. Wechsler, and Y. Ben-Zion (2009), Chemical and physical characteristics of pulverized Tejon Lookout granite adjacent to the San Andreas and Garlock faults: Implications for earthquake physics, *Pure Appl. Geophys.*, *166*, 1725–1746, doi:10.1007/s00024-009-0514-1.

Storti, F., A. Billi, and F. Salvini (2003), Particle size distributions in natural carbonate fault rocks: insights for non self-similar cataclasis, *Earth Planet. Sc. Lett.*, *206*, 173–186.

Wechsler, N., E. E. Allen, T. K. Rockwell, G. Girty, J. S. Chester, and Y. Ben-Zion (2011), Characterization of pulverized granitoids in a shallow core along the San Andreas Fault, Littlerock, CA, *Geophys. J. Int.*, *186*, 401–417, doi:10.1111/j.1365-246X.2011.05059.x.

Wilson, B., T. Dewers, Z. Reches, and J. Brune (2005), Particle size and energetics of gouge from earthquake rupture zones, *Nature*, *434*, 749–752, doi:10.1038/nature03433.

Woodcock, N. H., and K. Mort (2008), Classification of fault breccias and related fault rocks, *Geol. Mag.*, *145*, 435–440.

Yuan, F., V. Prakash, and T. Tullis (2011), Origin of pulverized rocks during earthquake fault rupture, *J. Geophys. Res.*, *116*, B06309, doi:10.1029/2010JB007721.

A. Billi, IGAG, Consiglio Nazionale delle Ricerche, c.o. Dipartimento Scienze della Terra, Sapienza Università di Roma, P.le A. Moro 5, 00185, Rome, Italy.

M.-L. Doan, Institut des Sciences de la Terre, Université Joseph Fourier, 1381 rue de la Piscine, F-38041 Grenoble CEDEX, France. (mai-linh.doan@obs.ujf-grenoble.fr)